

International Journal of Nanoelectronics and Materials

IJNeaM

ISSN 1985-5761 | E-ISSN 2232-1535



THz cut-off frequency of multilayer armchair graphene nanoribbon tunnel field-effect transistors

Taufik Syah Mauludin a, Maulana Ibrohim a, Dadi Rusdiana a, Lilik Hasanah a, Siti Kudnie Sahari b and Endi Suhendi a*

- ^aPhysics Study Program, Universitas Pendidikan Indonesia, Bandung (40154), Indonesia
- ^bFaculty of Engineering, Universiti Malaysia Sarawak, 94300 UNIMAS, Kota Samarahan, Sarawak, Malaysia
- *Corresponding author. Tel.: +62-815-6194-694; e-mail: endis@upi.edu

Received 01 December 2024, Revised 26 February 2025, Accepted 02 May 2025

ABSTRACT

Graphene nanoribbons with tunable energy bandgaps present notable advantages for tunneling field-effect transistor (TFET) applications. These nanoribbons, composed of carbon atoms arranged in a hexagonal lattice resembling a honeycomb structure, feature a narrow width. The cut-off frequency of TFETs reflects their potential for developing low-energy, high-frequency devices. This study employed the Airy function approach to model the cut-off frequency of multilayer armchair graphene nanoribbon (AGNR) TFETs. Numerical calculations were conducted using computational programming in Wolfram Mathematica. The TFET's potential profile was derived using the Airy function method to calculate transmittance, which was then used to determine the tunneling current through the Landauer equation and the Gauss-Legendre quadrature method. The tunneling current calculation enabled the estimation of the cut-off frequency. Results indicate that the cut-off frequency initially increases with gate voltage, reaches a peak, and subsequently decreases. Higher drain voltage and oxide thickness are associated with increased cut-off frequency, while longer channel lengths, wider multilayer graphene nanoribbons, and elevated temperatures tend to reduce it. Variations in AGNR layers significantly affect TFET performance, with trilayer AGNR TFETs achieving superior cut-off frequencies compared to their bilayer and monolayer counterparts.

Keywords: Multilayer armchair graphene nanoribbon, Cut-off frequency, Tunneling field-effect transistor, Airy function

1. INTRODUCTION

The International Technology Roadmap for Semiconductors (ITRS) has indicated that the scaling complementary metal-oxide-semiconductor (CMOS) transistors has reached a plateau, emphasizing the need to expand CMOS capabilities to further advance electronic systems [1]. CMOS technology is commonly used in most very large-scale integrated (VLSI) circuit chips, which can contain thousands or even millions of metal-oxidesemiconductor field-effect transistor (MOSFETs) [2]. An alternative for achieving high-speed, ultra-low-power, and energy-efficient devices is the tunneling field-effect transistor (TFET) [3], introduced by T. Baba in 1992. Unlike MOSFETs, TFETs utilize the quantum tunneling field effect at the barrier. They demonstrate superior energy efficiency compared to CMOS technology [4].

The cut-off frequency is a critical parameter for assessing transistor frequency behavior and intrinsic delay. A higher cut-off frequency results in reduced switching delays and enhances the high-frequency performance of TFET devices [5]. The cut-off frequency value indicates the advantage of TFETs in developing low-energy and high-frequency devices.

Graphene emerges as a promising material for TFETs due to

its exceptional properties. Graphene, composed of carbon atoms arranged hexagonally, exhibits high electron mobility exceeding 200,000 cm²/Vs [6]. While monolayer graphene was initially produced mechanically through methods like the scotch-tape technique [7], graphene can also be synthesized epitaxially via chemical vapor deposition (CVD) of hydrocarbons on metal substrates [8]. Even though the resulting material is multilayer graphene, it retains many of the attractive properties of monolayer graphene [9]. Stacked graphene layers exhibit distinct electronic structures based on layer number and stacking order [10], with the AB arrangement being the most common and stable [11]. Bilayer graphene arranged in a Bernal phase is more stable than AA-stacked configurations [12], and trilayer graphene stacked in a rhombohedral pattern can adjust its bandgap [13]. The rhombohedral stack is expected to have stronger electronic interaction compared to the Bernal stack.

Graphene nanoribbons (GNRs) are narrower than 10 nm function as transistors at room temperature, offering fast switching and high mobility [14]. These GNRs are categorized based on their edge type, with zigzag edges (ZGNRs) being metallic and armchair edges (AGNRs) exhibiting either semiconductor or metal properties [15]. GNR with adjustable energy bandgaps is beneficial for TFETs, enabling high-speed, low-power performance [16].

Many simulations have looked into TFET GNR traits [17–19], showing that GNRs with weak interlayer coupling are best for high-performance GNRFETs [20]. Additionally, introducing a lightly doped region between the drain and channel in GNR TFETs significantly enhances performance, reducing off-current by a factor of 10^2 – 10^3 , increasing on/off ratio by up to 10^5 , shortening delay times, reducing power-delay product (PDP), and diminishing drain-induced barrier thinning (DIBT) [21]. Simulation research is vital for optimizing electronic device performance before large-scale production.

This research focuses on modeling the cut-off frequency of AGNR multilayer TFETs using the Airy function approach to analyze multilayer AGNR TFET characteristics—monolayer (MAGNR), bilayer (BAGNR), and trilayer (TAGNR)—based on influential parameters. The Airy function solves the Schrödinger equation on TFETs, maintaining satisfactory precision compared to the Wentzel-Kramers-Brillouin (WKB) approximation [22], especially for low-energy tunneling probability calculations [23].

2. METHODS

In the low-energy approximation, the relationship between the dispersion energy E(k) to the wave vectors of monolayer graphene, bilayer graphene, and rhombohedral trilayer graphene is linear, quadratic, and cubic, respectively. The energy bandgap refers to the difference between the conduction band, labeled +E(k), and the valence band, marked labeled -E(k). The transverse momentum of AGNR is given by $k = n\pi/3w$. Table 1 shows the energy bandgap of multilayer graphene, where γ_1 representing the interlayer coupling at 0.39 eV [24], and v_f denotes the Fermi velocity. The width of GNR (w) is determined by the number of atoms along the AGNR width, which exhibits distinct properties [25].

All calculations were performed using Wolfram Mathematica 11.2 software. The potential profile of the TFET, determined by solving the Schrödinger equation [27], is calculated using the Airy function approach [23]. This method determines the electron transmittance, which represents the probability of electrons tunneling through the potential barrier from the source to the drain in the TFET structure. Subsequently, this transmittance is used to calculate the tunneling current through Equation (1), also known as Landauer's equation.

$$I_{d} = \frac{2q}{\pi h} \int_{E_{cc}}^{E_{Vs}} T(E) [f_{s}(E) - f_{d}(E)] dE$$
 (1)

where q is the electron charge, \hbar is the reduced Planck constant, T(E) is the electron transmittance, and $f_s(E)$ and $f_d(E)$ are the Fermi distributions on the source and drain in Equation (2).

$$f_s(E) = \frac{1}{1 + e^{\frac{E}{K_B T}}}; f_d(E) = \frac{1}{1 + e^{\frac{E + eV_d}{K_B T}}}$$
 (2)

where E is energy, KB is Boltzmann's constant and T is temperature [28].

Table 1. Energy dispersion and energy bandgap multilayer graphene nanoribbon [26]

Material	<u>+</u> E(k)	$\mathbf{E}_{\mathbf{g}}$	
Monolayer	ħ v _f k	$\frac{2\pi\hbar v_f}{3w}$	
Bilayer	$\frac{\hbar^2 v_f^2 k^2}{\gamma_1}$	$\frac{2\pi^2\hbar^2v_f^2}{9\gamma_1w^2}$	
Trilayer	$\frac{{\hbar}^3 {v_f}^3 k^3}{{{\gamma_1}^2}}$	$\frac{2\pi^{3}\hbar^{3}v_{f}^{3}}{27{\gamma_{1}}^{2}w^{3}}$	

The cut-off frequency is determined using Equation (3) [5], [17], [18], [29].

$$f_{t} = \frac{g_{m}}{2\pi C_{g}} \tag{3}$$

where g_m is the transconductance and C_g is the total capacitance at the gate. Transconductance represents the rate of change of the tunneling current concerning the gate voltage, as expressed in Equation (4).

$$g_{\rm m} = \frac{\partial I_{\rm d}}{\partial V_{\rm g}} \tag{4}$$

The total capacitance at the gate is an effect that arises due to the insulator layer, so that polarization occurs at the gate and the multilayer AGNR. The total capacitance at the gate, assuming a constant polarized charge, is shown in Equation (5).

$$C_{g} = \frac{2}{3}C_{ox}WL \tag{5}$$

where w is the width of the AGNR multilayer, L is the length of the AGNR multilayer at the gate, and $C_{\rm ox}$ is the capacitance in the oxidation region. This capacitance is calculated as the product of the dielectric constant $\epsilon_{\rm ox}/t_{\rm ox}$ where $\epsilon_{\rm ox}$ is the dielectric constant and $t_{\rm ox}$ is the oxide thickness. The cut-off frequency varies based on the drain voltage, channel length, oxide layer thickness, multilayer AGNR width, and temperature.

3. DISCUSSION AND RESULTS

The cut-off frequency is calculated using $V_d = 0.1~V$, w = 5.042~nm, L = 20~nm, $t_{ox} = 1~nm$, and T = 300~K, within a gate voltage range of 0.0~to~0.2~V. A low V_d helps maintain a balance between minimizing power consumption and maintaining reasonable current flow, crucial for low-power electronic applications like TFETs, which are designed to operate efficiently at low voltages. The channel length of 20~nm is a typical choice for nanoscale devices, reflecting modern scaling trends in semiconductor technology, where shorter channels enhance device switching speeds, but also increase leakage currents. A thin oxide layer ($t_{ox} = 1~nm$) is crucial for achieving strong electrostatic control over the channel, which is necessary for proper switching behavior in graphene-based devices. The thin oxide ensures that gate voltage efficiently modulates the channel.

As the gate voltage increases, the conduction band of the channel decreases until it falls below the valence band of the source. This leads to an increased probability of electrons tunneling towards the drain, resulting in a greater number of electrons moving from the source to the drain. The cut-off frequency rises until it reaches a maximum value, corresponding to an increase in transconductance, as shown in Figure 1. Subsequently, the cut-off frequency declines due to the combined effects of increased total capacitance, reduced carrier mobility induced by the gate field, and saturation of the tunneling current [30].

The peak cut-off frequency observed in TAGNR surpasses that of BAGNR and MAGNR, as shown in Table 2. This is attributed to the higher tunneling current in TAGNR compared to BAGNR and MAGNR. Moreover, the greater tunneling current in TAGNR causes the cut-off frequency value to decrease more rapidly after reaching its peak. The differences in cut-off frequency values between TAGNR and BAGNR are not substantial compared to those with MAGNR, likely because the bandgaps of TAGNR and BAGNR are similar to each other but different from those of MAGNR. Additionally, TAGNR exhibits the lowest threshold voltage compared to BAGNR and MAGNR due to its smaller bandgap, which requires less electron energy to traverse the potential barrier. The increased cut-off frequency leads to reduced switching delay and enhances the device's highfrequency performance [5].

3.1. Effect of Drain Voltage

The cut-off frequency is determined by adjusting the drain voltage to 0.05 V, 0.10 V, 0.15 V, 0.20 V, and 0.25 V. As shown in Figure 2, the cut-off frequency increases with rising drain voltage, exhibiting an exponential growth pattern. This increase is attributed to enhanced carrier mobility, leading to higher transconductance and a concurrent decrease in gate capacitance. The combination of reduced capacitive effects and elevated transconductance contributes significantly to the improvement of the cut-off frequency [30].

When comparing MAGNR, BAGNR, and TAGNR, it is evident that TAGNR consistently demonstrates a higher cut-off frequency across all drain voltage levels. This superior performance is due to stronger interlayer coupling in trilayer graphene, which enhances charge carrier mobility

Table 2. The peak cut-off frequency of the TFET multilayer AGNR

Material	Eg (eV)	V _g (V)	f (THz)
MAGNR	0.273	0.100	10.937
BAGNR	0.096	0.091	13.233
TAGNR	0.034	0.084	13.572

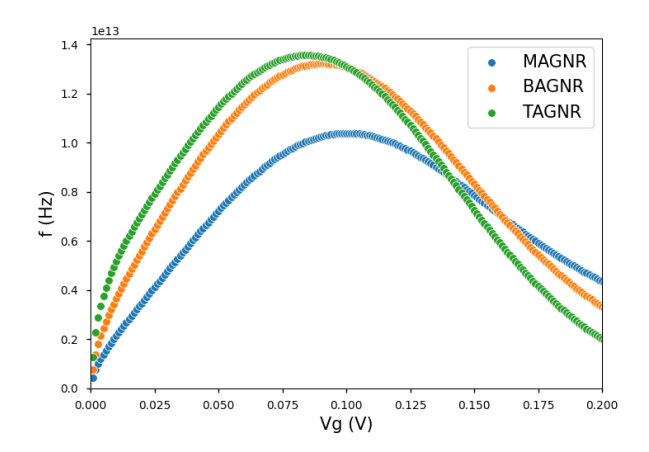


Figure 1. Cut-off frequency TFET multilayer AGNR

and reduces quantum capacitance effects. BAGNR, with its moderate interlayer coupling, shows improved performance compared to MAGNR but remains lower than TAGNR. MAGNR exhibits the lowest cut-off frequency due to limited interlayer interactions and reduced density of states, resulting in lower transconductance and higher gate capacitance.

Additionally, the threshold voltage tends to rise with increasing drain voltage, as depicted in Figure 3. This phenomenon is caused by the heightened potential barrier at the drain and enhanced gate-to-source coupling [31]. The threshold voltage shift is more pronounced in MAGNR compared to BAGNR and TAGNR due to the weaker electrostatic control in monolayer graphene. In contrast, TAGNR demonstrates better electrostatic integrity, leading to more stable threshold voltage characteristics under varying drain voltages.

Although increasing the drain voltage enhances the cut-off frequency, it is crucial to avoid excessively high values, as this may induce undesirable ambipolar currents in the off-state. To mitigate this risk, the drain voltage is maintained below the bandgap energy to prevent electron tunneling in

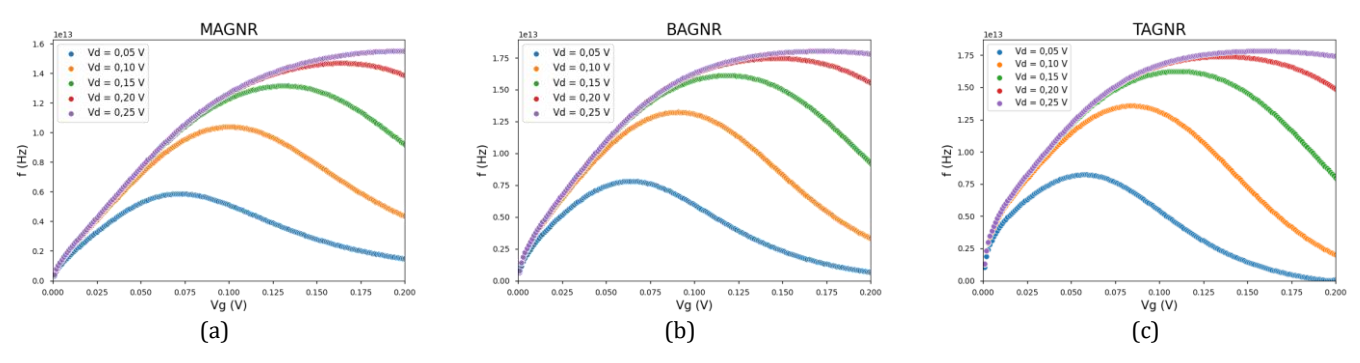


Figure 2. Effect of drain voltage on the cut-off frequency of the TFET: (a) MAGNR, (b) BAGNR, and (c) TAGNR

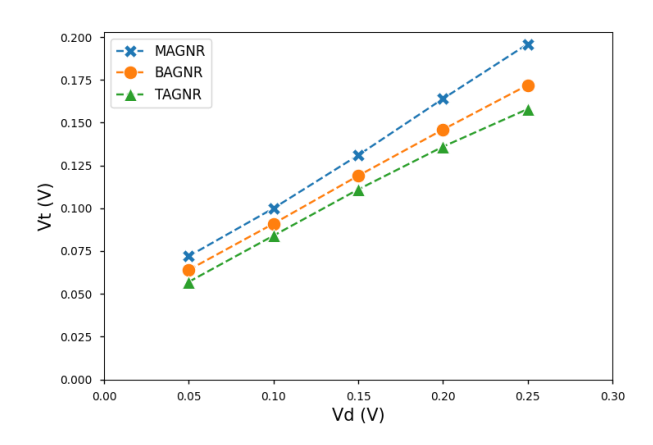


Figure 3. Effect of drain voltage on the threshold voltage of the TFET multilayer AGNR

the off-state. Exceeding the bandgap leads to the formation of a tunneling region at the channel-drain junction, increasing off-state leakage currents [32]. Moreover, higher drain voltages reduce the tunneling barrier, a phenomenon known as drain-induced barrier thinning (DIBT), which contributes to increased off-currents [33].

3.2. Effect of Channel Length

The length of the channel was adjusted to 10 nm, 15 nm, 20 nm, 25 nm, and 30 nm. Figure 4 illustrates that the cutoff frequency increases as the channel length decreases. This is because the gate capacitance diminishes linearly with decreasing channel length. A shorter channel length results in a reduced cross-sectional area. With less charge contained in the channel, more charge reaches the drain as it travels a shorter distance through the channel. Additionally, when the channel length is decreased, especially when it matches the thickness of the gate insulator, electrons move faster toward the drain due to a short-channel effect. As a result, the gate capacitance decreases.

Comparing MAGNR, BAGNR, and TAGNR, the cut-off frequency differs due to variations in interlayer coupling and carrier transport efficiency. MAGNR exhibits the highest cut-off frequency because of its minimal interlayer scattering and lower capacitance, resulting in faster charged

transport. BAGNR shows moderate performance, with increased interlayer interactions slightly reducing electron mobility compared to MAGNR. TAGNR, having stronger interlayer coupling and higher capacitance, demonstrates the lowest cut-off frequency among the three, as the additional layers introduce more resistance to carrier flow.

Channels that are 10 nm long are ideal for multilayer AGNR TFET because they have low resistance and capacitance, which can reduce delay. This short-channel effect can be further intensified by using a thinner dielectric thickness [34–36].

3.3. Effect of Thickness of Oxide Layer

The thickness of the oxide layer was adjusted to 0.5 nm, 1.0 nm, 1.5 nm, 2.0 nm, and 2.5 nm. Figure 5 illustrates that the cut-off frequency increases with an increase in the oxide layer thickness. Reducing the thickness of the oxide layer improves how the gate works, covering a wider range of energy and increasing the ability to store charge. The significant capacitance in a thin oxide layer leads to a lower cut-off frequency value. However, when the oxide layer thickness approaches or exceeds half of the channel length, a decrease in the cut-off frequency is observed [35, 37]. This happens because the gate voltage's electric field becomes less effective over longer distances. Consequently, there is a slight reduction in the channel's valence band, affecting the tunneling current, which becomes constrained by the narrower channel.

The gate oxide layer helps connect the gate and channel through capacitance, controlling the drain current in the TFET. Increasing the oxide layer thickness reduces the electrons generated in the drain as the forbidden depletion layer for electron occupation expands, diminishing the chance for electron penetration. Thinner gate oxide layers are preferred to operate the TFET for better stability, as demonstrated in previous studies [38]. Therefore, an oxide layer with a thickness of 0.5 nm can be considered the optimal parameter for multilayer AGNR TFET.

Comparing the effect of oxide thickness across MAGNR, BAGNR, and TAGNR TFETs reveals distinct behaviors. In MAGNR TFETs, the thinner oxide layer significantly enhances gate control due to stronger electrostatic

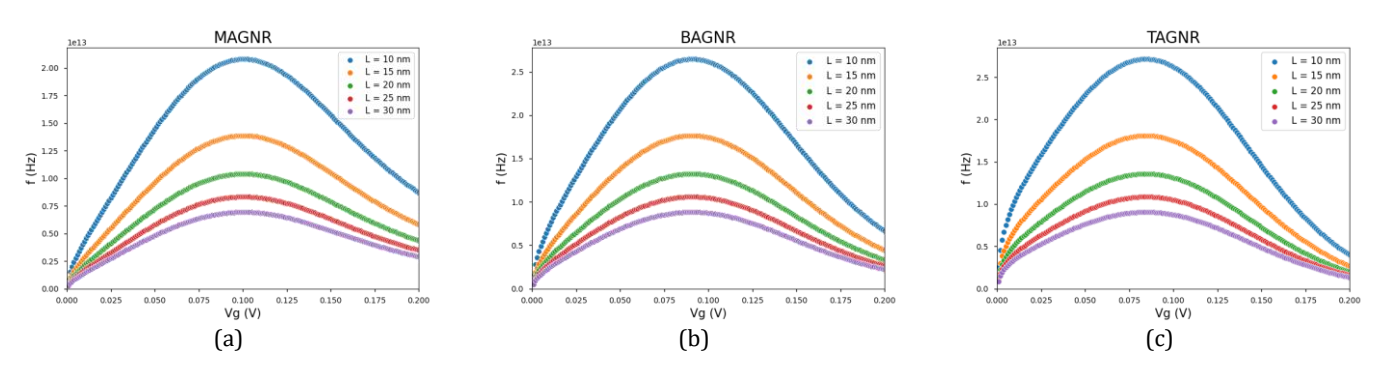


Figure 4. Effect of channel length on the cut-off frequency of the TFET: (a) MAGNR, (b) BAGNR, and (c) TAGNR

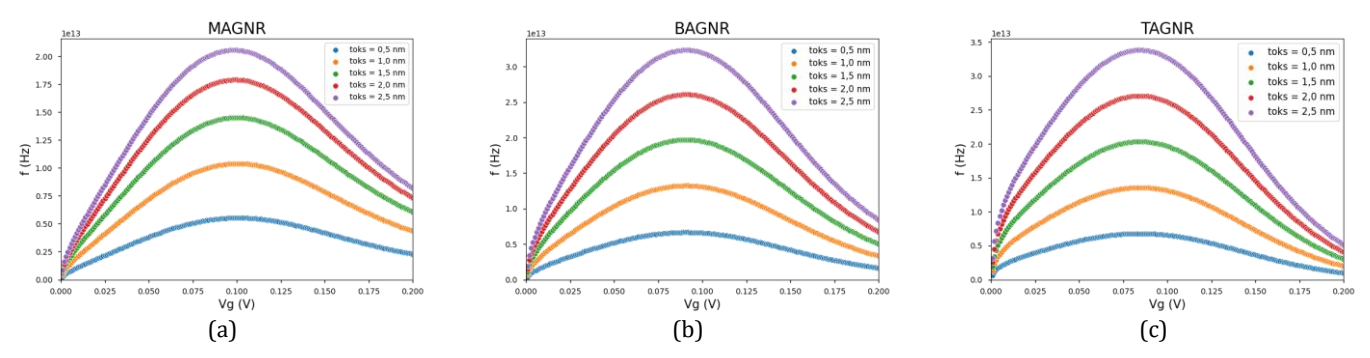


Figure 5. Effect of thickness of oxide layer on the cut-off frequency of the TFET: (a) MAGNR, (b) BAGNR, and (c) TAGNR

coupling, leading to higher cut-off frequencies. BAGNR exhibits moderate gate control, where the interlayer coupling introduces additional capacitance effects, slightly reducing the cut-off frequency compared to MAGNR. TAGNR TFETs, with more complex interlayer interactions, show the least sensitivity to oxide thickness variations, as the internal layers act as screening barriers, limiting the gate field's influence on the channel. This suggests that MAGNR TFETs are more suitable for high-frequency applications where oxide thickness optimization is critical, while TAGNR TFETs offer stability in performance despite oxide thickness variations.

3.4. Effect of Width

The width of the AGNR multilayer was varied to 1.353 nm, 3.197 nm, 5.042 nm, 7.256 nm, and 9.100 nm. In electronic applications that require ultra-thin materials and nanometer-scale devices, varying the width of graphene nanoribbons (GNRs) allows the device to operate across different power and frequency ranges. The narrower the GNR, the larger the energy bandgap it produces, significantly affecting the switching speed and energy efficiency of.

At larger widths, graphene approaches the properties of an intrinsic semiconductor without a bandgap, while at smaller widths, GNR behaves more like a semiconductor with a larger bandgap. A larger width for the multilayer AGNR leads to a decrease in the cut-off frequency. With an increase in the width of the multilayer AGNR, both the bandgap and effective mass decrease, resulting in a higher tunneling current [27]. A greater tunneling current leads to higher

transconductance. Meanwhile, a large multilayer AGNR width will produce a large quantum capacitance [39], causing the cut-off frequency to decrease as the multilayer AGNR width increases.

However, Figure 6 demonstrates that the lowest cut-off frequency value occurs when the width of the multilayer AGNR is 1.353 nm. This is because it's harder for electrons to move through the potential barrier when the bandgap of the multilayer AGNR is large, causing a decrease in the tunneling current.

The threshold voltage decreases when the AGNR multilayer width increases, as shown in Table 3. Achieving the threshold voltage occurs through tunneling from one band to another across a thin dielectric layer. A smaller bandgap, coupled with a reduced effective carrier mass, enables higher tunneling efficiency. Decreasing the threshold voltage results in lower power consumption, as it requires less power supply [40]. Decreasing the width of the AGNR multilayer widens the bandgap, leading to a notable decrease in off-state current and a reduction in on-state current due to the diminished low-energy subband. Opting for an extremely narrow bandwidth may not be advantageous, as it could result in a lower on-state current [39]. Therefore, a multilayer AGNR with a width of 3.197 nm is the optimal bandwidth for multilayer AGNR TFET.

The performance of multilayer AGNR TFETs is significantly influenced by the number of graphene layers. MAGNR exhibits the largest bandgap due to strong quantum confinement effects, leading to lower tunneling current and higher threshold voltage. Its high bandgap makes it suitable

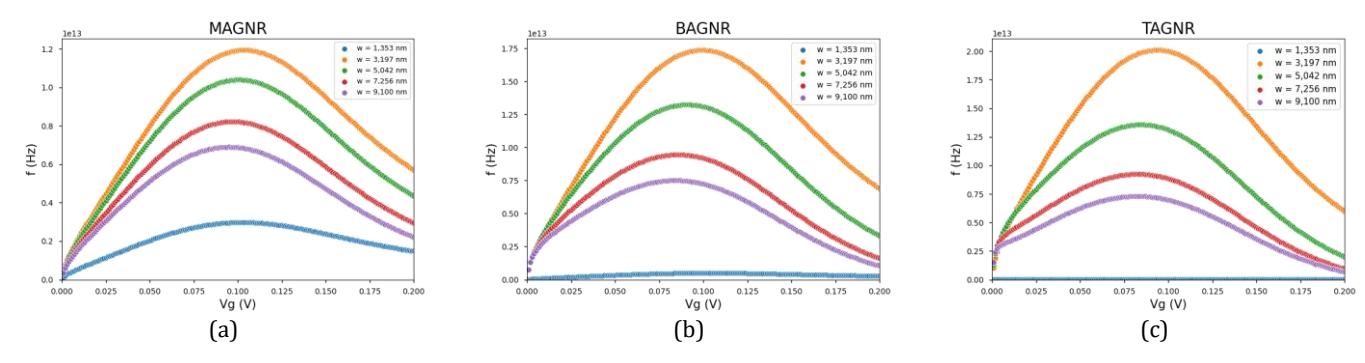


Figure 6. Effect of width of multilayer AGNR on the cut-off frequency of the TFET: (a) MAGNR, (b) BAGNR, and (c) TAGNR

Table 3. Effect of width of multilayer AGNR on the peak cut-off				
frequency of the TFET multilayer AGNR				

Material	W (nm)	N (atom)	E _g (eV)	V _g (V)	F (THz)
MAGNR	1.353	12	1.019	0.103	2.979
	3.197	27	0.431	0.102	11.943
	5.042	42	0.273	0.100	10.397
	7.256	60	0.190	0.097	8.222
	9.100	75	0.151	0.095	6.900
BAGNR	1.353	12	1.331	0.103	0.496
	3.197	27	0.238	0.099	17.364
	5.042	42	0.096	0.091	13.233
	7.256	60	0.046	0.086	9.451
	9.100	75	0.029	0.084	7.505
TAGNR	1.353	12	1.740	0.107	0.033
	3.197	27	0.132	0.094	20.108
	5.042	42	0.034	0.084	13.573
	7.256	60	0.011	0.082	9.241
	9.100	75	0.006	0.082	7.304

for ultra-low-power applications but limits high-frequency performance. BAGNR, on the other hand, shows a reduced bandgap compared to MAGNR, resulting in improved tunneling efficiency and higher on-state current. The interlayer coupling in BAGNR allows for more flexible bandgap tuning via external electric fields, making it suitable for balanced power and speed applications. TAGNR has the smallest bandgap among the three, which results in the highest tunneling current and the lowest threshold voltage. This configuration enhances transconductance and frequency performance but may increase leakage currents, thereby affecting energy efficiency. Understanding the trade-offs between these multilayer structures helps optimize TFET performance for specific electronic applications.

3.5. Effect of Temperature

The use of a temperature range from $100~\rm K$ to $500~\rm K$ in this study aims to evaluate the device's performance under various thermal conditions. In practical applications, semiconductor devices may operate across a wide range of temperatures, depending on the environment or specific application.

At lower temperatures, phonon scattering decreases, potentially enhancing carrier mobility. Conversely, at higher temperatures, increased phonon scattering may reduce mobility, impacting the device's overall efficiency. As depicted in Figure 7, the cut-off frequency decreases as the temperature increases. This reduction is due to the greater deviation in the Fermi distribution at elevated temperatures, leading to a decrease in the disparity between the Fermi distribution of the source and the channel. As a result, the tunneling current decreases because it becomes more difficult for electrons to flow from the source to the channel. High temperatures lead to low transconductance and charge mobility [41]. Elevated temperatures result in increased kinetic energy for charges, leading to random motion that disrupts carrier paths, thus reducing mobility. This random motion reduces the mobility of charges. The decreased charge mobility slows down the speed of charges, resulting in a lower tunneling current, which in turn leads to a smaller cut-off frequency.

comparing MAGNR, BAGNR, and temperature effects differ due to variations in their electronic structures and interlayer interactions. MAGNR exhibits the highest sensitivity to temperature changes because of its strong quantum confinement and absence of interlayer coupling. As temperature increases, the reduction in carrier mobility is more pronounced, leading to a steeper decline in cut-off frequency. BAGNR demonstrates moderate temperature sensitivity, where the presence of interlayer coupling helps mitigate the impact of phonon scattering to some extent, providing better stability in cutoff frequency compared to MAGNR. The bandgap tunability in BAGNR also influences its thermal response. TAGNR shows the least sensitivity to temperature variations due to stronger interlayer interactions and a more complex band structure that provides additional pathways for charge carriers. This structure maintains relatively higher carrier mobility at elevated temperatures, resulting in a more stable cut-off frequency compared to MAGNR and BAGNR.

As shown in Figure 8, the threshold voltage increases with temperature. Electrons can surpass the potential barrier when their energy exceeds the thermal energy threshold. At higher temperatures, electrons require more energy to overcome the potential barrier. Additionally, some electrons positioned slightly below the Fermi energy gain sufficient energy to transition to levels above the Fermi

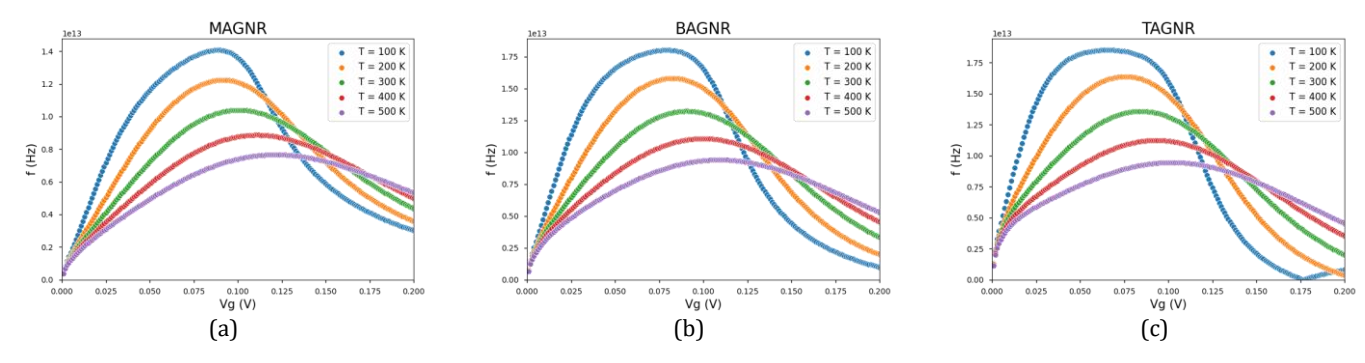


Figure 7. Effect of temperature on the cut-off frequency of the TFET: (a) MAGNR, (b) BAGNR, and (c) TAGNR

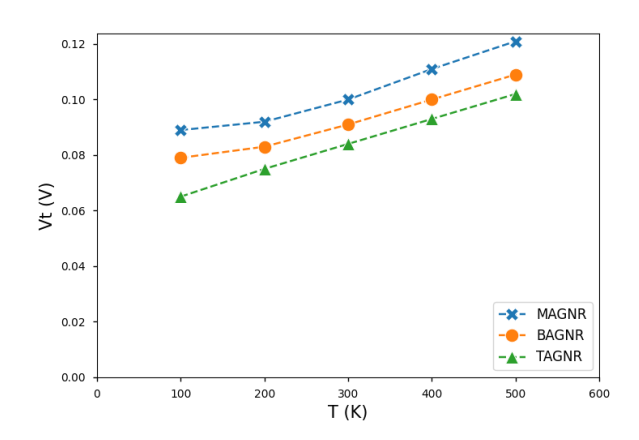


Figure 8. Effect of temperature on the threshold voltage of the TFET multilayer AGNR

energy, reducing the probability of finding electrons at energy levels lower than the Fermi level compared to low-temperature conditions.

4. CONCLUSION

The cut-off frequency increases with the gate voltage until it reaches a peak, after which it decreases. The impact of drain voltage and oxide thickness on the cut-off frequency are directly proportional. Conversely, the effects of channel length, multilayer AGNR width, and temperature are inversely related to the cut-off frequency. Trilayer AGNR TFET exhibits a superior cut-off frequency compared to its bilayer and monolayer counterparts.

ACKNOWLEDGMENTS

This work was financially supported by the "Hibah Penelitian Fundamental Reguler" Kementerian Pendidikan, Kebudayaan, Riset dan Teknologi Republik Indonesia Research Grants in the fiscal year 2023.

REFERENCES

- [1] M. Graef, "More Than Moore White Paper," in *2021 IEEE International Roadmap for Devices and Systems Outbriefs*, Nov. 2021, pp. 1–47, doi: 10.1109/IRDS54852.2021.00013.
- [2] R. J. Baker, *CMOS*. Hoboken, NJ, USA: John Wiley & Sons, Inc., 2010.
- [3] P. Tamak and R. Mehra, "Review on Tunnel Field Effect Transistors (TFET)," *International Research Journal of Engineering and Technology (IRJET)*, vol. 4, no. 7, pp. 1195–1200, 2017.
- [4] U. E. Avci, D. H. Morris, and I. A. Young, "Tunnel Field-Effect Transistors: Prospects and Challenges," *IEEE Journal of the Electron Devices Society*, vol. 3, no. 3, pp. 88–95, May 2015, doi: 10.1109/JEDS.2015.2390591.
- [5] S. Dash, G. S. Sahoo, and G. P. Mishra, "Improved Cutoff Frequency for Cylindrical Gate TFET Using Source Delta Doping," *Procedia Technology*, vol. 25, no. Raerest, pp. 450–455, 2016, doi: 10.1016/j.protcy. 2016.08.131.

- [6] K. I. Bolotin *et al.*, "Ultrahigh Electron Mobility in Suspended Graphene," *Solid State Communications*, vol. 146, no. 9–10, pp. 351–355, Jun. 2008, doi: 10.1016/j.ssc.2008.02.024.
- [7] A. K. Geim, "Graphene: Status and Prospects," *Science*, vol. 324, no. 5934, pp. 1530–1534, Jun. 2009, doi: 10.1126/science.1158877.
- [8] A. K. Geim and K. S. Novoselov, "The Rise of Graphene," *Nature Materials*, vol. 6, no. 3, pp. 183–191, Mar. 2007, doi: 10.1038/nmat1849.
- [9] K. S. Novoselov, V. I. Fal'ko, L. Colombo, P. R. Gellert, M. G. Schwab, and K. Kim, "A Roadmap for Graphene," *Nature*, vol. 490, no. 7419, pp. 192–200, Oct. 2012, doi: 10.1038/nature11458.
- [10] K. F. Mak, J. Shan, and T. F. Heinz, "Electronic Structure of Few-Layer Graphene: Experimental Demonstration of Strong Dependence on Stacking Sequence," *Physical Review Letters*, vol. 104, no. 17, p. 176404, Apr. 2010, doi: 10.1103/PhysRevLett.104. 176404.
- [11] J. Paul Nery, M. Calandra, and F. Mauri, "Ab-Initio Energetics of Graphite and Multilayer Graphene: Stability of Bernal Versus Rhombohedral Stacking," *2D Materials*, vol. 8, no. 3, p. 035006, Jul. 2021, doi: 10.1088/2053-1583/abec23.
- [12] A. V. Rozhkov, A. O. Sboychakov, A. L. Rakhmanov, and F. Nori, "Electronic Properties of Graphene-Based Bilayer Systems," *Physics Reports*, vol. 648, pp. 1–104, Aug. 2016, doi: 10.1016/j.physrep.2016.07.003.
- [13] M. Koshino, "Interlayer Screening Effect in Graphene Multilayers with ABA and ABC Stacking," *Physical Review B*, vol. 81, no. 12, p. 125304, Mar. 2010, doi: 10.1103/PhysRevB.81.125304.
- [14] X. Li, X. Wang, L. Zhang, S. Lee, and H. Dai, "Chemically Derived, Ultrasmooth Graphene Nanoribbon Semiconductors," *Science*, vol. 319, no. 5867, pp. 1229–1232, Feb. 2008, doi: 10.1126/science. 1150878.
- [15] G. Liang, N. Neophytou, D. E. Nikonov, and M. S. Lundstrom, "Performance Projections for Ballistic Graphene Nanoribbon Field-Effect Transistors," *IEEE Transactions on Electron Devices*, vol. 54, no. 4, pp. 677–682, Apr. 2007, doi: 10.1109/TED.2007.891872.
- [16] Q. Zhang, T. Fang, H. Xing, A. Seabaugh, and D. Jena, "Graphene Nanoribbon Tunnel Transistors," *IEEE Electron Device Letters*, vol. 29, no. 12, pp. 1344–1346, Dec. 2008, doi: 10.1109/LED.2008.2005650.
- [17] E. Suhendi, J. Brajadenta, A. Aminudin, and D. Rusdiana, "Modelling of Cut-off Frequency of Armchair Graphene Nanoribbon Tunnel Field Effect Transistor Using Transfer Matrix Method," International Journal of Nanoelectronics and Materials, vol. 16, no. 3, pp. 441–448, 2023.
- [18] E. Suhendi, L. Hasanah, F. A. Noor, and N. Kurniasih, "Modeling of Armchair Graphene Nanoribbon Tunnel Field Effect Transistors for Low Power Applications," *Journal of Semiconductor Technology and Science*, vol. 19, no. 4, pp. 336–346, Aug. 2019, doi: 10.5573/ JSTS.2019.19.4.336.
- [19] E. Suhendi, R. Syariati, F. A. Noor, N. Kurniasih, and Khairurrijal, "Simulation of Dirac Electron Tunneling

- Current in Armchair Graphene Nanoribbon Tunnel Field-Effect Transistors Using a Transfer Matrix Method," *Advanced Materials Research*, vol. 1112, no. November, pp. 128–132, 2015, doi: 10.4028/www.scientific.net/amr.1112.128.
- [20] Y. Ouyang, H. Dai, and J. Guo, "Projected Performance Advantage of Multilayer Graphene Nanoribbons as a Transistor Channel Material," *Nano Research*, vol. 3, no. 1, pp. 8–15, Jan. 2010, doi: 10.1007/s12274-010-1002-8.
- [21] S. S. Ghoreishi, K. Saghafi, R. Yousefi, and M. K. Moravvej-Farshi, "Graphene Nanoribbon Tunnel Field Effect Transistor with Lightly Doped Drain: Numerical Simulations," *Superlattices and Microstructures*, vol. 75, pp. 245–256, Nov. 2014, doi: 10.1016/j.spmi.2014.07.042.
- [22] A. J. Smith and A. R. Baghai-Wadji, "A Numerical Technique for Solving Schrödinger's Equation in Molecular Electronic Applications," in *Smart Structures, Devices, and Systems IV*, Dec. 2008, vol. 7268, p. 72681Q, doi: 10.1117/12.814318.
- [23] F. Oktasendra, "Pengaplikasian Metode Fungsi Airy pada Permasalahan Probabilitas Terobosan Kuantum," Simetri, vol. 2, no. 2, pp. 75–80, 2016.
- [24] A. H. Castro Neto, F. Guinea, N. M. R. Peres, K. S. Novoselov, and A. K. Geim, "The Electronic Properties of Graphene," *Reviews of Modern Physics*, vol. 81, no. 1, pp. 109–162, Jan. 2009, doi: 10.1103/RevModPhys. 81.109.
- [25] K. Wakabayashi, M. Fujita, H. Ajiki, and M. Sigrist, "Electronic and Magnetic Properties of Nanographites," in *Carbon Based Magnetism*, vol. 59, no. 12, Elsevier, 2006, pp. 279–304.
- [26] Y. J. Lee, "UC Riverside UC Riverside Electronic Theses and Dissertations," *UC Riverside*, pp. 1–152, 2022.
- [27] C. S. P. Bimo, F. A. Noor, M. Abdullah, and Khairurrijal, "A Theoretical Model of Band-to-Band Tunneling Current in an Armchair Graphene Nanoribbon Tunnel Field-Effect Transistor," *Advanced Materials Research*, vol. 896, pp. 371–374, Feb. 2014, doi: 10.4028/www.scientific.net/AMR.896.371.
- [28] Q. Cheng, "Modeling and Simulation of Nano-Scale Transistor," 2022.
- [29] W. V. Devi and B. Bhowmick, "Optimisation of Pocket Doped Junctionless TFET and Its Application in Digital Inverter," *Micro & Nano Letters*, vol. 14, no. 1, pp. 69–73, Jan. 2019, doi: 10.1049/mnl.2018.5086.
- [30] S. K. Vishvakarma, A. Beohar, V. Vijayvargiya, and P. Trivedi, "Analysis of DC and Analog/RF Performance on Cyl-GAA-TFET Using Distinct Device Geometry," *Journal of Semiconductors*, vol. 38, no. 7, p. 074003, Jul. 2017, doi: 10.1088/1674-4926/38/7/074003.
- [31] P. Kumari, S. Dash, and G. P. Mishra, "Impact of technology scaling on analog and RF performance of

- SOI-TFET," *Advances in Natural Sciences: Nanoscience and Nanotechnology*, vol. 6, no. 4, 2015, doi: 10.1088/2043-6262/6/4/045005.
- [32] N. Dang Chien, C.-H. Shih, Y.-H. Chen, and N. T. Thu, "Increasing drain voltage of low-bandgap tunnel field-effect transistors by drain engineering," in 2016 International Conference on Electronics, Information, and Communications (ICEIC), Jan. 2016, pp. 1–4, doi: 10.1109/ELINFOCOM.2016.7562947.
- [33] D. Haehnel, I. A. Fischer, A. Hornung, A.-C. Koellner, and J. Schulze, "Tuning the Ge(Sn) Tunneling FET: Influence of Drain Doping, Short Channel, and Sn Content," *IEEE Transactions on Electron Devices*, vol. 62, no. 1, pp. 36–43, Jan. 2015, doi: 10.1109/TED.2014.2371065.
- [34] S. Saurabh and M. J. Kumar, *Fundamentals of Tunnel Field-effect Transistors*. Taylor & Francis Group, LLC, 2017.
- [35] R. Cheng *et al.*, "High-frequency Self-aligned Graphene Transistors with Transferred Gate Stacks," *Proceedings of the National Academy of Sciences*, vol. 109, no. 29, pp. 11588–11592, Jul. 2012, doi: 10.1073/pnas.1205696109.
- [36] J. Chauhan and J. Guo, "Assessment of High-frequency Performance Limits of Graphene Field-effect Transistors," *Nano Research*, vol. 4, no. 6, pp. 571–579, Jun. 2011, doi: 10.1007/s12274-011-0113-1.
- [37] H.-F.Xu, J. Cui, W. Sun, and X.-F. Han, "Analysis of Non-uniform Hetero-gate-dielectric Dual-material Control Gate TFET for Suppressing Ambipolar Nature and Improving Radio-frequency Performance," *Chinese Physics B*, vol. 28, no. 10, p. 108501, Sep. 2019, doi: 10.1088/1674-1056/ab3a8b.
- [38] K. Sivasankaran and P. S. Mallick, "Impact of Parameter Fluctuations on RF Stability Performance of DG Tunnel FET," *Journal of Semiconductors*, vol. 36, no. 8, p. 084001, Aug. 2015, doi: 10.1088/1674-4926/36/8/084001.
- [39] B. Rawat and R. Paily, "Performance Evaluation of Bilayer Graphene Nanoribbon Tunnel FETs for Digital and Analog Applications," *IEEE Transactions on Nanotechnology*, vol. 16, no. 3, pp. 411–416, May 2017, doi: 10.1109/TNANO.2017.2675939.
- [40] G. Kaur, G. Singh, and M. Kaur, "Double Gate Heterostructure Based Tunnel FET with 51.5 mV/decade Subthreshold Slope," *IOSR Journal of VLSI and Signal Processing*, vol. 06, no. 05, pp. 53–59, May 2016, doi: 10.9790/4200-0605015359.
- [41] M. Akbari Eshkalak, "Graphene nano-ribbon field effect transistor under different ambient temperatures," *Iranian Journal of Electrical and Electronic Engineering*, vol. 12, no. 2, pp. 147–153, 2016.